Assessment of Numerical Simulations of Deep Circulation and Variability in the Gulf of Mexico Using Recent Observations

STEVEN L. MOREY,[a,b] GANESH GOPALAKRISHNAN,[c] ENRIC PALLÁS SANZ,[d]
JOAO MARCOS AZEVEDO CORREIA DE SOUZA,[d,e] KATHLEEN DONOHUE,[f] PAULA PÉREZ-BRUNIUS,[d]
DMITRY DUKHOVSKOY,[b] ERIC CHASSIGNET,[b] BRUCE CORNUELLE,[c] AMY BOWER,[g]
HEATHER FUREY,[g] PETER HAMILTON,[h] AND JULIO CANDELA[d]

[a] *Florida Agricultural and Mechanical University, Tallahassee, Florida*
[b] *Florida State University, Tallahassee, Florida*
[c] *Scripps Institution of Oceanography, University of California, San Diego, La Jolla, California*
[d] *Centro de Investigacion Cientifica y de Educacion Superior de Ensenada, Ensenada, Baja California, Mexico*
[e] *MetOcean Solutions, New Plymouth, New Zealand*
[f] *University of Rhode Island, Narragansett, Rhode Island*
[g] *Woods Hole Oceanographic Institution, Woods Hole, Massachusetts*
[h] *North Carolina State University, Raleigh, North Carolina*

ABSTRACT

Three simulations of the circulation in the Gulf of Mexico (the ''Gulf'') using different numerical general circulation models are compared with results of recent large-scale observational campaigns conducted throughout the deep (>1500 m) Gulf. Analyses of these observations have provided new understanding of large-scale mean circulation features and variability throughout the deep Gulf. Important features include cyclonic flow along the continental slope, deep cyclonic circulation in the western Gulf, a counterrotating pair of cells under the Loop Current region, and a cyclonic cell to the south of this pair. These dominant circulation features are represented in each of the ocean model simulations, although with some obvious differences. A striking difference between all the models and the observations is that the simulated deep eddy kinetic energy under the Loop Current region is generally less than one-half of that computed from observations. A multi-decadal integration of one of these numerical simulations is used to evaluate the uncertainty of estimates of velocity statistics in the deep Gulf computed from limited-length (4 years) observational or model records. This analysis shows that the main deep circulation features identified from the observational studies appear to be robust and are not substantially impacted by variability on time scales longer than the observational records. Differences in strengths and structures of the circulation features are identified, however, and quantified through standard error analysis of the statistical estimates using the model solutions.

1. Introduction

The purpose of this study is to assess the ability of present-day numerical model simulations of the Gulf of Mexico (GoM) to simulate prominent features of the deep-layer circulation in the GoM as characterized by recent observational studies. With few exceptions, models of the GoM have primarily focused on simulating and forecasting the upper ocean circulation. Because assessment and verification efforts have also focused on the upper ocean, it is uncertain how accurately these models simulate the deep circulation in their present

configurations. To address this knowledge gap, the deep circulation simulated by three different free-running, or non-data-assimilative, simulations are compared with each other and with recent large-scale observational campaigns. The three models are chosen since they are commonly applied for state estimation and forecasting of the GoM circulation.

The GoM circulation is dominated by the Loop Current (LC), a branch of the North Atlantic Ocean western boundary current system that enters the Gulf of Mexico through the Yucatan Strait, loops anticyclonically, and exits through the Straits of Florida. This unstable current exhibits a cycle of northward penetration into the GoM, separation of anticyclonic rings or eddies

Corresponding author: Steven L. Morey, steven.morey@famu.edu

that drift generally westward, and subsequent retraction to the south (Vukovich 2007). These baroclinic circulation features are confined to waters above the base of the main thermocline, or roughly the upper 800–1000 m, and thus the GoM behaves much like a two-layer system (Hurlburt and Thompson 1980) with the lower layer exhibiting nearly vertically coherent flow (Hamilton 1990, 2009). The LC and the anticyclonic eddies are very energetic features with current speeds that can exceed $2 \, m \, s^{-1}$. Because of the importance of the LC and eddies to oil and gas activities in the northern GoM and the relative ease of monitoring them (primarily with satellites due to their strong sea surface height and, in the cold months, sea surface temperature expression), a large number of studies have been conducted to understand the dynamics and forecasting of these upper-layer circulation features in the GoM.

Historically, much less attention has been paid to the circulation of the deep layer of the GoM, primarily due to challenges of collecting long-term measurements with good spatial sampling at these depths. Over the past two decades, though, interest in the deep GoM has increased with the advancement of oil and gas operations off the continental shelf into waters deeper than 1000 m. The measurement of current speeds exceeding $1 \, m \, s^{-1}$ near the seabed at 2000-m depth along the base of the Sigsbee Escarpment (Fig. 1) in 1999 (Hamilton and Lugo-Fernandez 2001; Nowlin et al. 2001) led to a number of studies of this potentially energetic environment. These mainly focused on modeling the deep currents near this steep bathymetric feature in the northwestern GoM at depths between 1500 and 3000 m. Hamilton and Lugo-Fernandez (2001) characterized the strong currents along this escarpment as having features similar to topographic Rossby waves (TRWs). Over the western slope of the Bay of Campeche, Kolodziejczyk et al. (2011) also reported TRW-like motions from current-meter observations, though less energetic than over the steeper Sigsbee Escarpment. Hamilton (2007) used ray tracing techniques to deduce the origin of TRWs impacting the northeastern part of the Sigsbee Escarpment to be the western edge of the LC. Dukhovskoy et al. (2009) and Morey and Dukhovskoy (2013) developed a high-resolution (<1-km horizontal grid spacing and <15-m vertical grid spacing near the sea floor) model that simulated these features with traits similar to observations and suggested that the origins of strong currents along the escarpment differ from the shallower northeastern part and the deeper part to the southwest. Their simulations revealed that energetic motions along the northeastern Sigsbee Escarpment arrive from the vicinity of the Mississippi Fan to the east when the LC is extended, consistent with Hamilton (2007), and that

lower-layer eddies traveling westward across the deep basin impact the southwestern portion of the escarpment.

Observations of energetic flows in the deep GoM have motivated recent studies aimed at identifying and understanding origins of the energy in the deep GoM. For example, Oey (2008) diagnosed model results to suggest a connection between the deep circulation and the LC variability. Donohue et al. (2016b) analyzed observational data to demonstrate a baroclinic instability mechanism for exciting eddies in the deep layer under the LC. In the western GoM, Tenreiro et al. (2018) suggested a coupling between propagating LC eddies and deep circulation features due to compression and stretching of the lower layer inducing relative vorticity changes through potential vorticity conservation. Most recently, Hamilton et al. (2019) explained the connection between the origins of the deep-layer energy and other parts of the deep GoM through radiation of TRWs.

Unlike the upper-layer circulation, there is only a limited understanding of the characteristics of the deep circulation throughout the entire deep GoM due to the lack of large-scale long-term observational studies. Hamilton (1990) synthesized historic data from nine moorings deployed at various times in the 1980s for durations of a few months to a little over a year to describe low-frequency TRW motions in the deep GoM. Further analyses of TRWs using data from more extensive deep moorings were performed by Hamilton (2009). DeHaan and Sturges (2005) analyzed historic hydrographic data, following Hofmann and Worley (1986), and profiling drifters at 900 m to provide evidence of the existence of a mean cyclonic flow around the perimeter of the deep GoM. It is worth noting that analysis of current-meter measurements from deep moorings show that the upper- and deep-layer flows are separated at approximately this depth (Sheinbaum et al. 2007).

Because a comprehensive depiction of the deep GoM circulation from observations has been previously lacking, it has not been possible to assess the simulation of deep currents in models over the basin as a whole. Recently, groundbreaking observational campaigns have provided the first opportunity to evaluate numerical models over the entire deep GoM, a necessary step for using these models to synthesize observations and provide new understanding of the dynamics of the GoM, including upper layer–deep layer coupling. These observational programs include a 4-yr Lagrangian study using a large number of drifters in the lower layer (Hamilton et al. 2016b; Pérez-Brunius et al. 2018) and, under the LC region, a dense array of moorings and inverted echo sounders with pressure gauges (PIES; Donohue et al. 2016a). In addition, an array of full-depth moorings in the western Gulf of Mexico has been

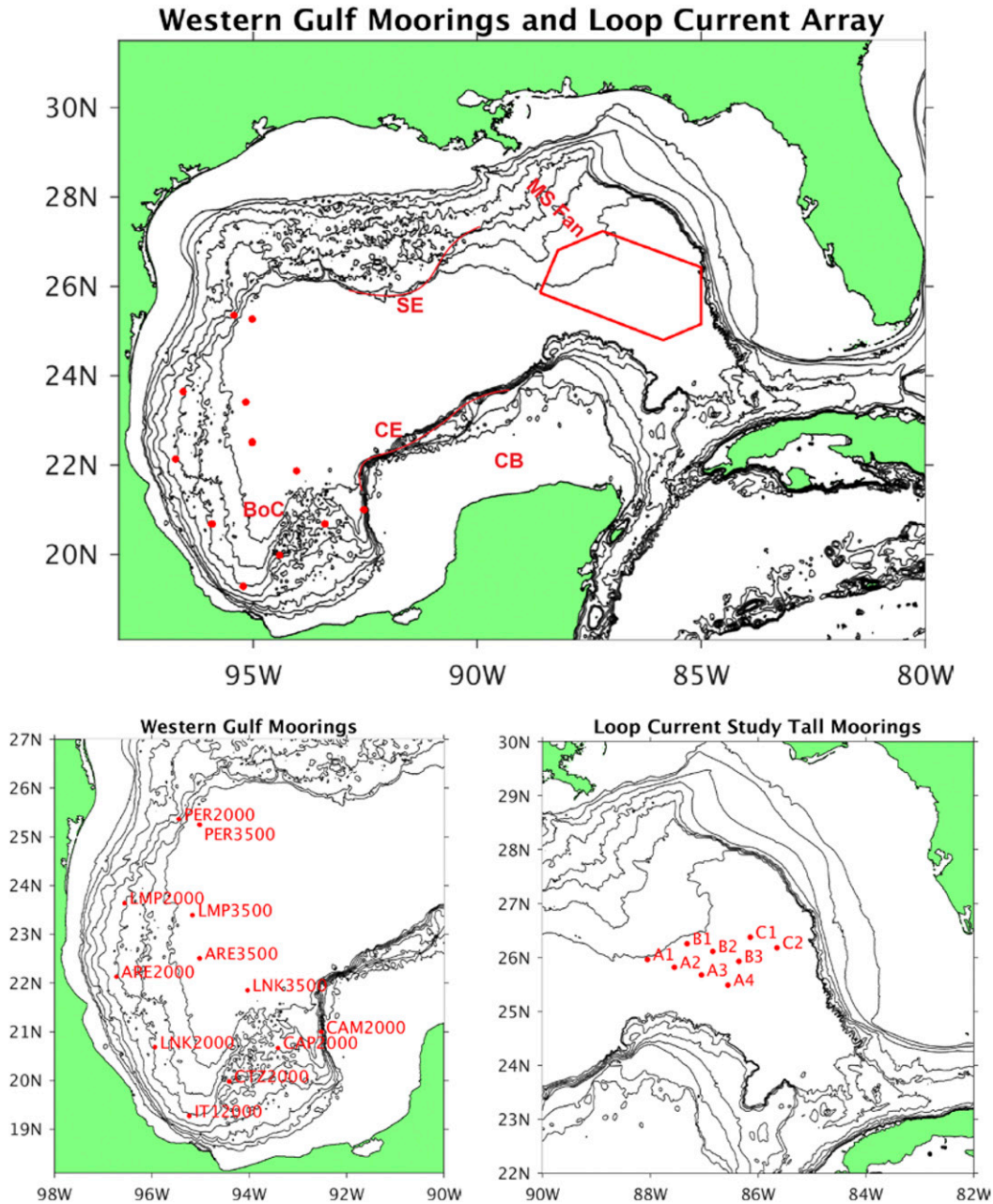## Western Gulf Moorings and Loop Current Array

FIG. 1. (top) Locations of the Loop Current Study mooring array (region bounded by the red polygon) and western GoM moorings (red dots): MS Fan = Mississippi Fan, BoC = Bay of Campeche, CB = Campeche Bank, SE = Sigsbee Escarpment, and CE = Campeche Escarpment. (bottom left) Expanded view of the western GoM showing mooring locations and identifiers. Isobaths are contoured at 100, 200, and every 500 m between 500 and 3000 m in this and subsequent figures. (bottom right) Locations of the Loop Current Study tall moorings.

operated by the Centro de Investigación Científica y Educación Superior de Ensenada (CICESE) over the last decade.

The new understanding gained from these observational studies allows for the first time an evaluation of how well numerical models are simulating the basic characteristics of the deep GoM circulation. Aspects of

the models or their configurations that could be impact the lower-layer circulation include vertical coordinate system (geopotential-following, terrain-following, isopycnal-following, etc.), vertical and horizontal grid resolution, effective resolution of the bathymetry (determined by bathymetry smoothing and resolution of the horizontal grid), hydrographic characteristics (water mass

representation, stratification), lateral boundary conditions, and numerical methods and parameterizations. Though a comprehensive assessment of these traits is not the purpose of this study, this paper presents an evaluation of the model representation of major features of the deep circulation simulated by three different existing GoM models/configurations that are commonly used for forecasting and scientific studies. Additionally, one of these is a multidecadal (54 years) simulation (Dukhovskoy et al. 2015) that is analyzed over multiple distinct time segments to evaluate the representativeness of the basic characteristics of the deep GoM circulation determined from shorter length (several years) observational programs.

2. Data and methods

a. Observations and analyses

This study compares statistical analyses of simulated velocity from three numerical models with analyses of observational data from the deep GoM. Specifically, the observational data are from a set of current-meter moorings in the western GoM and two recent studies of the deep circulation in the GoM. These studies include a basinwide Lagrangian study (Hamilton et al. 2016b; Pérez-Brunius et al. 2018) and a study of the deep circulation under the LC region using moored current meters and PIES (Hamilton et al. 2014, 2016a).

The basinwide Lagrangian study of the deep circulation described by Hamilton et al. (2016b) involved 152 acoustically tracked RAFOS floats, 121 ballasted at 1500 m and 31 ballasted at 2500 m, and 6 RAFOS-equipped APEX profiling floats with parking depth at 1500 m. The data span the roughly 4-yr period from July 2011 through June 2015. The floats recorded their positions three times per day, as determined from four sound source moorings. Pérez-Brunius et al. (2018) analyzed these data to produce the first maps of mean deep currents from observations in the GoM (Fig. 2). Given the near uniformity of currents with depth below 1000 m (Hamilton 1990), the 1500- and 2500-m floats were analyzed collectively to produce the gridded maps. Specifically, Pérez-Brunius et al. (2018) averaged the float velocities daily within $0.5° \times 0.5°$ overlapping boxes centered on a $0.25° \times 0.25°$ grid. Statistics (e.g., mean velocity, eddy kinetic energy) were then computed from these binned velocity data.

The second recent observational program used here provided a four-dimensional mapping of currents and density structure under the LC region from a high-density array of moored instruments over a 2.5-yr period (May 2009–November 2011) (Hamilton et al. 2014, 2016a; hereinafter referred to as the Loop Current Study). This

array consisted of 25 PIES; 9 full-depth tall moorings with temperature, conductivity, and velocity measurements; and 7 near-bottom current-meter moorings deployed under the LC region (Fig. 1). Velocity time series from the moored current meters at 2000-m depth are filtered with a 40-h low-pass Lanczos kernel and decimated to 6-h intervals prior to analysis. The PIES acoustic travel time data were converted to synthetic temperature and salinity profiles using historical hydrography (Hamilton et al. 2014). Three-dimensional mappings of these data were used to produce mapped baroclinic velocity profiles, from which the absolute geostrophic velocities were computed using the deep current-meter measurements. The complete procedure for producing these mapped velocity fields is described in Hamilton et al. (2014) and Donohue et al. (2016b).

Velocity observations from 12 moorings in the western Gulf of Mexico along the 2000- and 3500-m isobaths (Fig. 1) operated by the "CANEK" group provide long data records for assessing the variability of deep currents in this region. Velocity data from the moorings include measurements from downward-looking Teledyne RDI LongRanger 75-kHz (LR75) and WorkHorse 600-kHz (WH600) acoustic Doppler current profilers (ADCPs) and single-point Doppler current meters deployed between summer–autumn 2008 and spring 2017. A schematic of a typical configuration of the deep CANEK-group moorings can be found in Pallàs-Sanz et al. (2016).

Data from the moorings are vertically interpolated to 1500-m depth for analysis and comparison with model solutions. Interpolation at these depths is appropriate as the velocity is vertically coherent (see, e.g., Kolodziejczyk et al. 2012; Tenreiro et al. 2018) and most of the moorings have a single-point current meter near 1500 m. No statistically significant differences are found if the analysis is performed using interpolation to different depths between 1400 and 1800 m. The velocity time series are smoothed using a binomial filter prior to interpolation to 1-hourly intervals to avoid aliasing. The time series are analyzed for the 4-yr period from 6 August 2012 to 6 August 2016, because these moorings have nearly continuous measurements during this time period (~1460 days) with the exception of LNK3500 (1101 days) and PER3500 (867 days).

b. Numerical simulations

The numerical simulations used in this study are based on the Massachusetts Institute of Technology general circulation model (MITgcm), the Regional Ocean Modeling System (ROMS), and the Hybrid Coordinate Ocean Model (HYCOM). These simulations are all free-running versions of their data assimilative counterparts that are commonly used for producing ocean
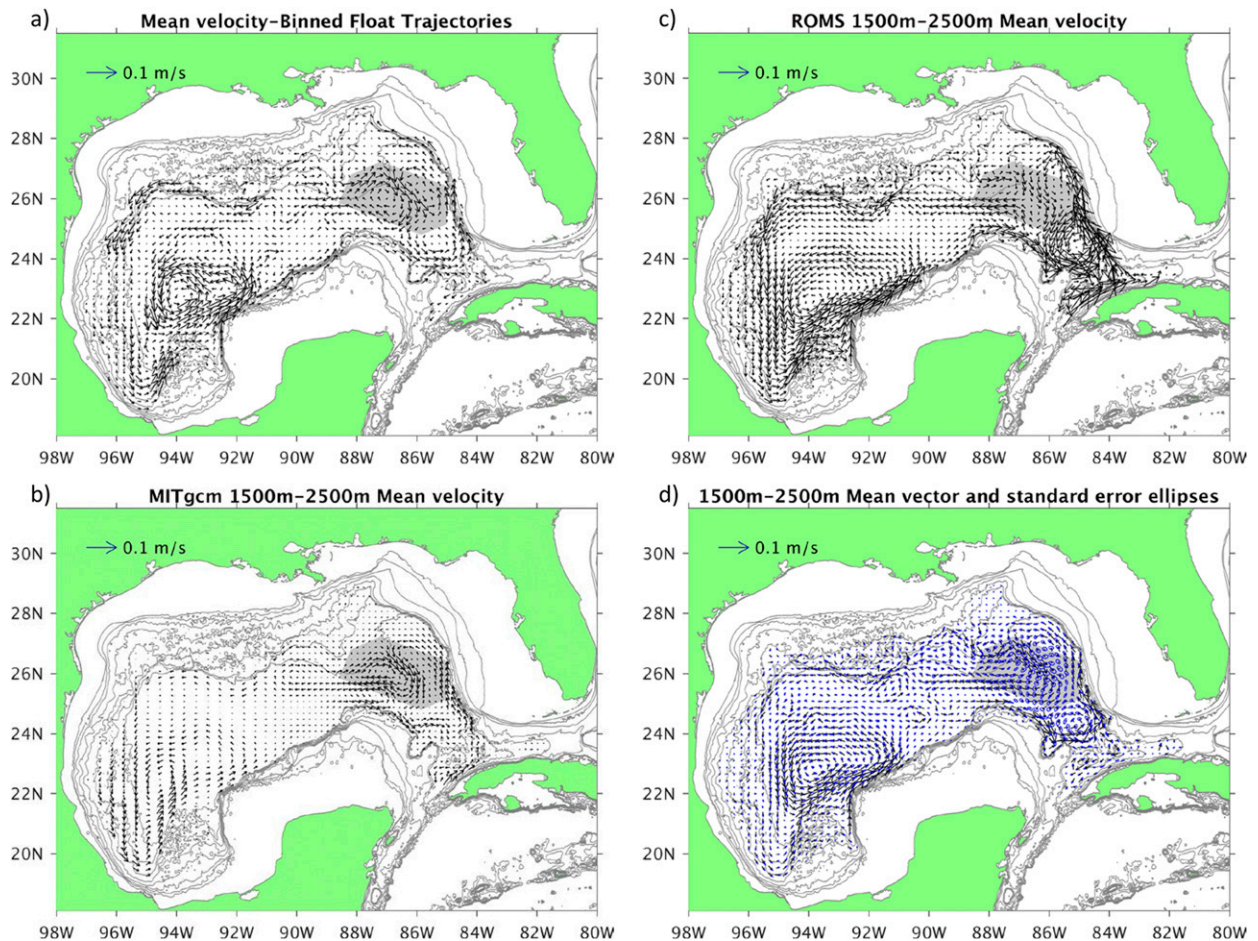
FIG. 2. (a) Mean velocity from mapped RAFOS float data computed by Pérez-Brunius et al. (2018). The shaded region indicates the location of the Loop Current Study mooring array (used in Fig. 6, below). Also shown are maps of the mean 1500–2500-m depth-averaged velocity from (b) 4-yr MITgcm, (c) 4-yr ROMS, and (d) 52-yr HYCOM simulation output. Blue ellipses around the arrowheads in (d) indicate the standard error of the mean velocity from thirteen 4-yr intervals. Model vectors are shown every fourth grid point for MITgcm and every fifth grid point for ROMS and HYCOM.

analyses, reanalyses, and forecasts. As these simulations are not constrained by data assimilation, their LC behavior and eddy fields do not necessarily match the "real ocean" for any given date. Rather, these stochastic circulation features evolve based on the nonlinear model dynamics and forcing (lateral boundary and surface).

1) MITGCM

A free-running simulation of the GoM circulation based on the MITgcm (MITgcm-GoM) was run for this study. The MITGCM (Marshall et al. 1997) integrates the primitive (Navier–Stokes) equations on a sphere under the Boussinesq approximation. It has been applied for GoM state estimation, forecasting, and adjoint sensitivity studies (e.g., Gopalakrishnan et al. 2013a,b; Hoteit et al. 2013; Rudnick et al. 2015; Gopalakrishnan et al. 2019).

The MITgcm–GoM model was originally developed for state estimation and prediction of the upper ocean circulation in the GoM, including LC evolution and eddy shedding. For these purposes, satellite-derived ocean surface observations and subsurface in situ observations are assimilated using a four-dimensional variational (4DVAR) method. For this study, however, no data assimilation is performed. The model domain extends from 8.5° to 31°N and from 98° to 72.5°W, covering the GoM, part of the Caribbean Sea, and the Gulf Stream. The model uses a telescopic grid with a horizontal resolution of $1/20° \times 1/20°$ in the central GoM which decreases to $1/10° \times 1/10°$ toward the boundaries and western part of the domain. The vertical grid is composed of 80 z levels. The model topography for the GoM basin is from the GoMRI high-resolution ($1/100° \times 1/100°$) topography, version 2.0, and ETOPO2

TABLE 1. Numerical parameters and methods used in model simulations.

ROMS	
Horizontal spacing	5 km
Vertical coordinates	(36) S-coordinate [modified as in Souza et al. (2015)]
Quadratic bottom drag coef	0.003
Scalar horizontal advection	Multidimensional positive definite advection transport algorithm (Smolarkiewicz and Grabowski 1990)
Horizontal momentum advection	Third-order upwind
Horizontal viscosity	Smagorinsky
Vertical turbulence	Mellor–Yamada level 2.5
Tides	TPXO 7.1
MITgcm	
Horizontal spacing	$(1/20)°–(1/10)°$
Vertical coordinates	80 z levels (with partial cells)
Quadratic bottom drag coef	0.002
Scalar horizontal advection	Third-order direct space time
Horizontal momentum advection	Third-order direct space time
Horizontal viscosity	Laplacian, $10 \, \mathrm{m^2 \, s^{-1}}$ + Biharmonic, $1 \times 10^{10} \, \mathrm{m^4 \, s^{-4}}$
Vertical turbulence	K-profile parameterization
Tides	None
HYCOM	
Horizontal spacing	Mercator grid: 0.04° in lon by 0.04° cos(lat) in lat
Vertical coordinates	20 hybrid layers
Quadratic bottom drag coef	0.0022
Scalar horizontal advection	Second-order flux-corrected transport
Horizontal momentum advection	Second-order flux-corrected transport
Horizontal viscosity	Max[background Laplacian ($0.002 \, 86 \, \mathrm{m \, s^{-1}}$), Smagorinsky] + biharmonic ($0.02 \, \mathrm{m \, s^{-1}}$)[a]
Vertical turbulence	K-profile parameterization
Tides	None

[a] Biharmonic and Laplacian coefficients are diffusive velocities and are multiplied by the grid spacing (cubed for biharmonic mixing; Chassignet and Garraffo 2001).

topography is used for the rest of the model domain. The vertical z-level spacing is 2.5 m at the surface, and the spacing of the 80 levels gradually increases to 100 m at the maximum bottom depth of 4000 m. In this configuration, the model is run in hydrostatic mode with an implicit free surface (see Table 1 for additional model parameters).

This simulation uses initial conditions (initialized on 1 January 2009) and boundary conditions interpolated from the HYCOM global 1/12° analysis (http://hycom.org/dataserver/glb-analysis) with Navy Coupled Ocean Data Assimilation (NCODA; Chassignet et al. 2007; Metzger et al. 2014). The model open boundaries are set at 31°N and 72.5°W, with horizontal velocity relaxation over a buffer zone with 1° width and with 1–5-day relaxation time scale. No tidal or atmospheric pressure forcing is applied. The simulation is forced with the National Centers for Environmental Prediction (NCEP)–National Center for Atmospheric Research reanalyses (R1; Kalnay et al. 1996) 6-hourly air temperature, specific humidity, zonal and meridional wind speed, precipitation, and short- and longwave radiative fluxes. Monthly climatological freshwater fluxes from riverine sources are prescribed using data from the Estimating the Circulation and

Climate of the Ocean (ECCO) global model (Stammer et al. 2002). The upper ocean circulation from this free-running circulation is assessed in Gopalakrishnan et al. (2013a). For this study, daily output from the simulation for the four years forced by atmospheric and lateral boundary condition data from 2009 to 2012 are analyzed.

With the telescopic horizontal grid spacing gradually increasing from 5 km in the central GoM to 10 km toward the boundaries, the MITgcm–GOM has the lowest resolution of the three model configurations used in this study. This model solution is therefore expected to be generally smoother and weaker than the observations and the other two models. Given the past emphasis on application to upper ocean circulation, the model representation of the deep circulation has not been optimized by adjustments of horizontal resolution, vertical gridding, mixing scheme, or topography.

2) ROMS

The Regional Ocean Modeling System (ROMS) is a three-dimensional primitive equation ocean model with hydrostatic and Boussinesq approximations (Shchepetkin and McWilliams 2005, 2009; Haidvogel et al. 2008).

The ROMS model uses a modified terrain-following vertical coordinate that provides the ability to increase resolution near the surface and bottom boundary layers. A modification of this scheme described by Souza et al. (2015) is used in the present application.

ROMS is configured for the GoM using a grid with ~5-km horizontal resolution and 36 vertical layers. The bathymetry combines data from the General Bathymetric Chart of the Oceans (GEBCO), corrected (particularly in the southern and western GoM) with data from the U.S. National Oceanic and Atmospheric Administration (NOAA), proprietary data from PEMEX (Petróleos Mexicanos), and other observations collected during several cruises performed by CICESE. Spurious velocities associated with erroneous horizontal pressure gradients are a common issue for terrain-following vertical coordinate models such as ROMS. Smoothing of the model bathymetry is therefore necessary, which can lead to a misrepresentation of areas of strong slope. To minimize this problem a linear programing-based smoothing of the bathymetry (Sikirić et al. 2009) is applied interactively to areas with spurious velocities of magnitude $1 \, \mathrm{cm \, s^{-1}}$ or larger that develop in an at-rest simulation. Additional model parameters are given in Table 1.

Initial and daily lateral boundary conditions are interpolated from the Global Eddy Permitting Ocean Reanalysis (GLORYS) 2 v3 from Mercator Ocean. The ROMS simulation is forced with hourly atmospheric fields from the NCEP Climate Forecast System Reanalysis (CFSR; Saha et al. 2010). Discharge from 41 rivers to the GoM was prescribed using USGS data for U.S. rivers and a daily climatology for the Mexican rivers (J. Zavala 2016, personal communication). Since the GLORYS reanalysis does not include tidal circulation, 11 constituents obtained from the Oregon State University TOPEX/Poseidon Global Inverse Solution tidal model (TPXO 7.1; Egbert and Erofeeva 2002) are introduced as a separate spectral forcing (daily means are analyzed largely filtering the tidal variability). Although this simulation was initially developed to provide the background solution for a 4DVAR data assimilative run to generate an ocean reanalysis for the GoM, 4 yr of daily mean outputs from the free-running simulation are analyzed in this work. The model circulation at 1500 m has been assessed using velocity measurements from moorings and Lagrangian observations by Maslo et al. (2020) and the upper ocean, including the LC, has been verified by Estrada-Allis et al. (2020).

3) HYCOM

HYCOM solves the non-Boussinesq primitive equations on a generalized (hybrid) vertical coordinate system

that allows vertical coordinates to follow isopycnal layers in the stratified ocean and transition to pressure-following (z level) or terrain-following coordinates in unstratified and shallow areas. HYCOM has been developed for use in ocean prediction systems by a partnership of institutions as a U.S. component to the Global Ocean Data Assimilation Experiment (GODAE; Chassignet et al. 2009). It forms the basis for analysis and prediction systems for the NOAA and U.S. Navy and has been used extensively by the scientific community.

Dukhovskoy et al. (2015) performed a multidecadal (54 years) free-running simulation using a configuration of this model similar to the configuration of the Naval Research Laboratory GoM Nowcast/Forecast System. The model domain spans from 18.9° to 31.96°N and from 98° to 76.4°W with horizontal resolution of 1/25° longitude by [cos(latitude)/25]°, or approximately 3.8–4.2-km grid spacing (Table 1). This model configuration has 20 vertical layers using the HYCOM hybrid vertical coordinates (a visualization of these layers can be found in Dukhovskoy et al. 2015).

The simulation is initialized from a 5-yr spinup run that started from rest with the Generalized Digital Environmental Model 3.0 (GDEM) climatological fields. Open boundary conditions are derived from a semi-monthly climatology produced by a 1/12°-resolution North Atlantic HYCOM simulation. Following spinup, surface forcing for the simulation is computed from hourly atmospheric variables from the CFSR for the period 1992–2009 and no tidal forcing is applied. This 18-yr period of atmospheric forcing is repeated three times to produce a 54-yr simulation. Dukhovskoy et al. (2015) show that this model realistically represents the stochastic LC cycle and eddy propagation pathways, and that there is no similarity in the LC and eddy field between 18-yr cycles for the same atmospheric forcing dates.

The first 52 years of this simulation are put into 13 subsets of nonoverlapping 4-yr segments for analysis. Because the model states are very different for the same forcing dates over the three cycles of atmospheric forcing, estimates of statistics computed from the 13 segments are considered independent. Thus, standard errors for the estimates of the statistics can be computed from these independent estimates. Analysis of this multidecadal simulation in this manner yields information on the representativeness of statistical properties of the deep circulation derived from observational programs conducted over shorter periods of several years.

c. Model data analysis

The horizontal velocity (u and v denoting eastward and northward components) from the three model simulations at daily intervals (instantaneous daily fields

for the MITgcm and HYCOM simulation, and daily mean fields for the ROMS) are analyzed at 1500-m depth (for comparison with western GoM moorings), 2000-m depth (for comparison with mapped velocity and current-meter moorings from the Loop Current Study array), and vertically averaged over 1500–2500-m depth for comparison with mapped Lagrangian velocities. It should be noted that the mean velocities computed from Lagrangian data have both spatial and temporal averaging, as they are binned over 0.5° (in latitude and longitude) regions. Hamilton et al. (2019) show that these mean velocities are generally smaller in magnitude than those from single point (current meter) measurements.

From the model velocity time series at each model grid point, mean velocity vectors $(\overline{u}, \overline{v})$ are computed over 4-yr record lengths (one 4-yr record from the MITgcm and ROMS simulations, and 13 nonoverlapping 4-yr records from the HYCOM simulation). Standard deviation ellipses from these velocity time series are computed from their principal axes following Emery and Thomson (2004) for comparison with western GoM mooring data. Kinetic energy (KE) spectra are also compared between the model velocity time series and current-meter records at the western GoM and Loop Current Study moorings. The spectra are computed in variance preserving form as $0.5 \times$ frequency $\times (S_{uu} + S_{vv})$, where S_{uu} and S_{vv} are the autospectra for the eastward and northward velocity components.

The kinetic energy per unit mass of the mean flow [termed the mean kinetic energy (MKE) in Pérez-Brunius et al. (2018)] (Fig. 3) is computed as

$$\text{MKE} = (\overline{u}^2 + \overline{v}^2)/2. \tag{1}$$

The eddy kinetic energy per unit mass (EKE; Fig. 4) is computed for each model gridpoint velocity time series (of length N days) as

$$\text{EKE} = \frac{1}{N}\sum_{i=1}^{N}\frac{[(u_i - \overline{u})^2 + (v_i - \overline{v})^2]}{2}. \tag{2}$$

In contrast to the significant differences in mean velocity computed from binned Lagrangian versus single-pint observations, Pérez-Brunius et al. (2018) show that velocity variance (and hence EKE) computed from these different measurements are more similar. The ratio of the MKE to the total kinetic energy, MKE/(MKE + EKE) (Fig. 5), gives an indication of the persistence of the mean circulation.

The standard deviation ellipses computed from the 13 HYCOM estimates of the mean velocity provide the standard errors of the statistics. EKE is a nonnegative quantity and thus not normally distributed, so the standard deviation from the estimates computed from the multiple segments cannot strictly be considered as the standard error. However, inspection of the EKE estimates reveals they approximately follow Gaussian distributions over much of the region. Skewness (Pearson's moment coefficient of skewness) and kurtosis (excess kurtosis) are calculated for the 13 EKE estimates at each model grid point. The area mean and standard deviation of the skewness and kurtosis computed over all grid points with mean values greater than $10\,\text{cm}^2\,\text{s}^{-2}$ are 0.03 ± 0.49 and −0.53 ± 0.72, respectively. These values lie within a commonly acceptable range of zero for considering the distributions to be normal (Gravetter and Wallnau 2014). Therefore, at each point, the standard deviations computed from the 13 EKE estimates are used as proxies for the standard errors to represent the uncertainty of EKE computed from 4-yr records.

3. Results

a. Deep circulation features from observations

Major features of the deep GoM circulation identified from the recent observational data analyzed in previous publications are summarized here for comparison to the numerical simulations.

Analysis of deep Lagrangian observations (Hamilton et al. 2016b) by Pérez-Brunius et al. (2018) confirms the existence of a mean cyclonic flow around the rim of the basin (Fig. 2) that had been previously suggested by analysis of hydrographic data (e.g., Hofmann and Worley 1986; DeHaan and Sturges 2005) and moored current-meter observations (Tenreiro et al. 2018). Other notable features not previously well documented are a cyclonic deep gyre in the southwestern GoM (termed the Sigsbee Abyssal Gyre) and a dipole of counterrotating cells in the mean velocity field under the LC region in the eastern GoM (centered at approximately 26°N). There is also suggestion of a mean cyclonic flow to the south of this dipole. Inspection of the mean deep velocity from the Loop Current Study (Hamilton et al. 2014) also supports the existence of a complex structure of counterrotating cells in the LC region (a dipole), similar to that seen from the analysis of the Lagrangian data (Fig. 6).

Analyses of the MKE (Fig. 3a) and EKE (Fig. 4a) show a clear distinction in the eastern and western parts of the basin. The eastern part of the basin exhibits higher EKE than the west while the western part generally has higher mean kinetic energy than the east (Figs. 3–5). Miron et al. (2019) also analyzed these RAFOS float data and demonstrated that the deep GoM is divided
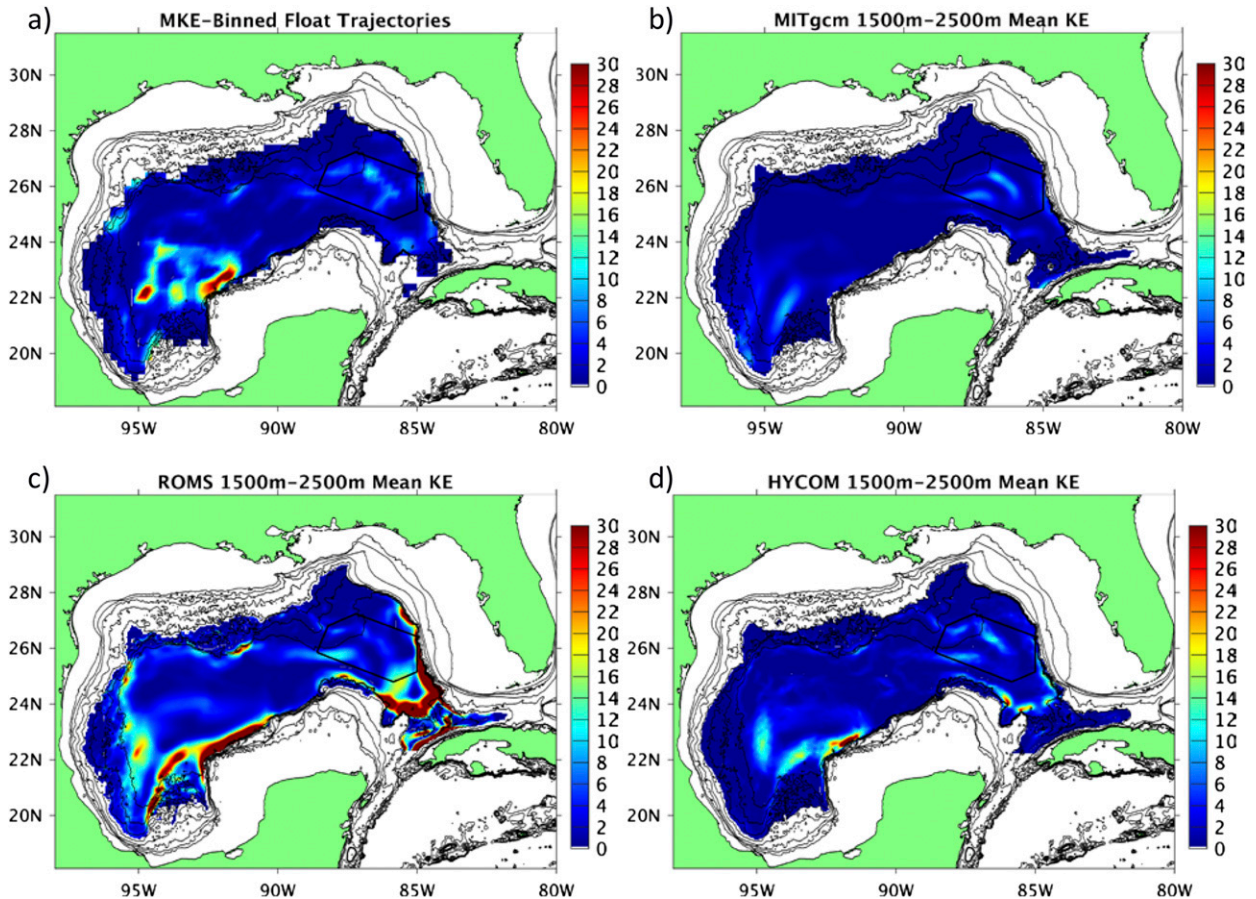
FIG. 3. (a) MKE (cm^2 s^{-2}) derived from the binned RAFOS float velocities by Pérez-Brunius et al. (2018). Also shown are maps of MKE computed from the (b) MITgcm, (c) ROMS, and (d) HYCOM simulations.

into two regions of near equal areas separated by a roughly meridional boundary. These regions have residence times of 4.5 (western) and 3.5 (eastern) yr, with communication restricted to a slow cyclonic circulation that is well constrained by f/h (potential vorticity) contours in the western basin. This deep Lagrangian circulation geography differs from its surface counterpart, indicating distinct connectivity characteristics with important consequences for the transport of potential pollutants and/or biological material.

b. Mean circulation

Inspection of the mean 1500–2500-m depth-averaged velocity field from the three models (4 years of model output for the MITgcm and ROMS simulations, and the 52 years for the HYCOM simulation) reveals similarity to the mean circulation derived from the mapped Lagrangian observations (Fig. 2). Each model generally produces a cyclonic flow around the rim of the basin, the cyclonic Sigsbee Abyssal Gyre, and a dipole of recirculating anticyclonic–cyclonic cells in the area of the

Loop Current Study mooring array. Additionally, all models show a cyclonic circulation to the south of this dipole. Analyses of the 1500, 2500, and 1500–2500-m depth-averaged model velocity fields are very similar, consistent with the reported coherence of the deep currents by Hamilton (1990).

There are, however, some significant differences among the model solutions and between the models and the float velocities. Most notable are differences in the magnitudes of the mean velocity associated with some of the major circulation features. This is illustrated by maps of the MKE (Fig. 3), which is proportional to the square of the magnitude of the mean velocity [Eq. (1)]. The MITgcm simulation generally has weaker mean circulation in the lower layer than the other models and that computed from the Lagrangian observations, with the exception of the circulation features under the LC region, which are comparable to observations. This model's mean cyclonic flow around the rim of the deep GoM also appears to be interrupted, or at least much weaker in magnitude, in the
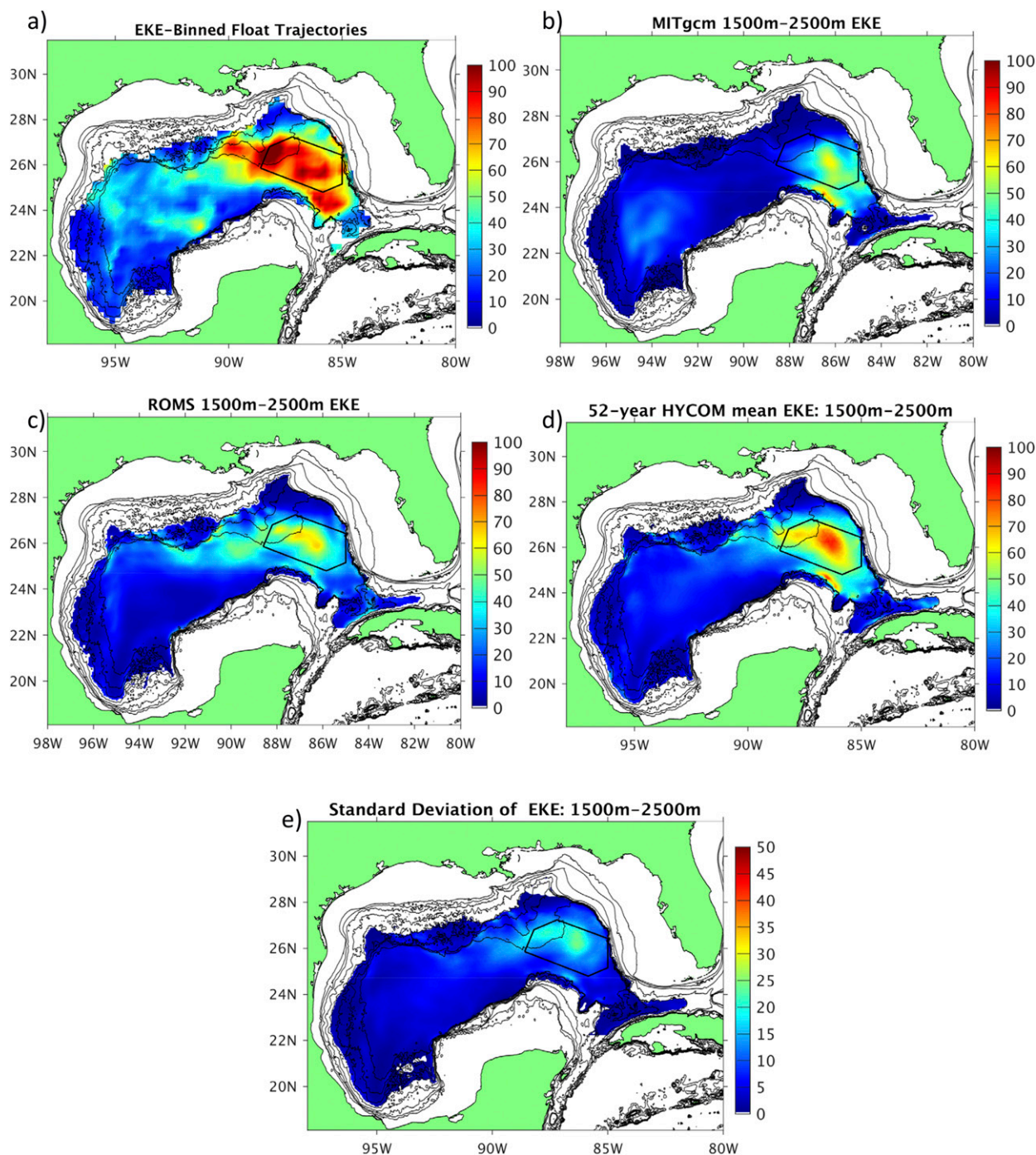
FIG. 4. (a) EKE (cm^2 s^{-2}) derived from the binned RAFOS float velocities by Pérez-Brunius et al. (2018). Also shown are maps of EKE computed from the (b) MITgcm, (c) ROMS, and (d) HYCOM simulations. (e) Standard error (computed as standard deviation from thirteen 4-yr records) of EKE estimates from HYCOM (note the different range of the color bar). The EKE for HYCOM shown in (d) is the mean of the thirteen 4-yr EKE estimates from that simulation.

northwestern part of the basin and along the Campeche Escarpment.

The ROMS simulation produces the strongest mean velocities of all models, particularly around the continental

slope where the model mean velocities are substantially stronger than those inferred from Lagrangian observations. As with the MITgcm simulation, an exception is the strength of the dipole under the LC region, which is also
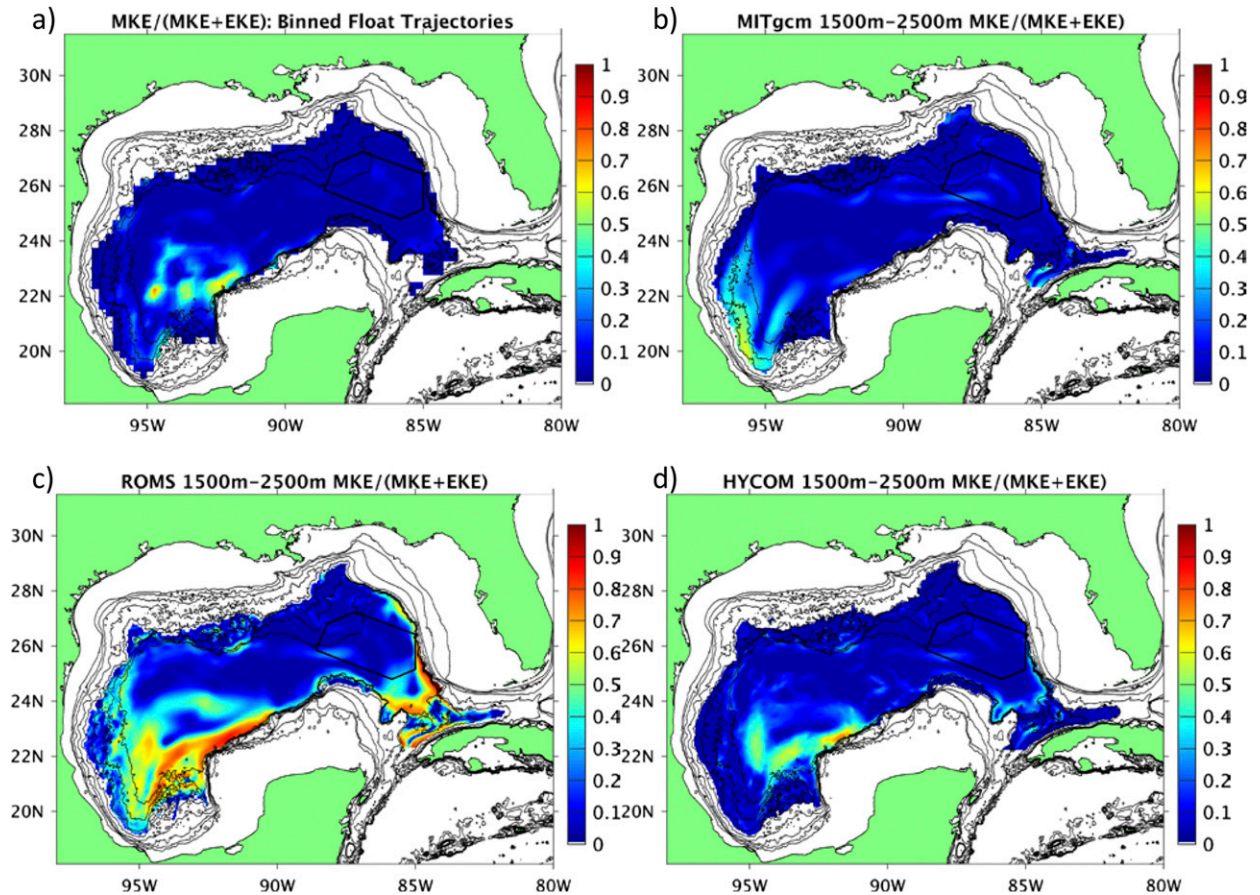
FIG. 5. (a) Ratio of MKE to the total kinetic energy per unit mass [MKE/(MKE + EKE)] derived from the binned RAFOS float velocities by Pérez-Brunius et al. (2018). Also shown are maps of the ratio of MKE to total kinetic energy computed from the (b) MITgcm, (c) ROMS, and (d) HYCOM simulations.

of comparable magnitude to the Lagrangian observations. The cyclone to the south of this dipole feature is notably strong, which may be due to it being a recirculation of the cyclonic deep boundary current. This boundary current is much stronger in the ROMS simulation than the other models and the observations, particularly along the southern and eastern part of the basin. The stronger currents over the deep topographic slope may be in part a consequence of the well-known numerical errors that can occur in computing the pressure gradient terms over sloping bathymetry in models with terrain-following coordinates, even though ROMS has numerical options to partially mitigate this (e.g., Shchepetkin and McWilliams 2003). The MKE of the Sigsbee Abyssal Gyre is of similar magnitude to that computed from the float trajectories, but this feature in the model seems to extend southward and westward throughout the deep Bay of Campeche, whereas the observations show a distinct separation between this feature and the boundary current along the slope to its south and west.

Like the MITgcm and ROMS simulations, the HYCOM simulation has similar mean velocity magnitudes in the lower-layer circulation features under the LC region as the mapped Lagrangian observations. This dipole therefore appears to be a robust feature in the mean velocity field that is well represented in all the model simulations. The boundary current is also of similar magnitude to the observations, except weaker in the northwestern part of the basin and along the Campeche Escarpment between approximately 91° and 88°W, similar to the MITgcm solution. This model is the only of the three analyzed here that produces a mean Sigsbee Abyssal Gyre that exhibits separation from the continental slope of the western and southern Bay of Campeche. Inspection of individual 4-yr mean velocity maps from the HYCOM simulation (not shown) reveals a consistent separation of the gyre from the continental slope in each.

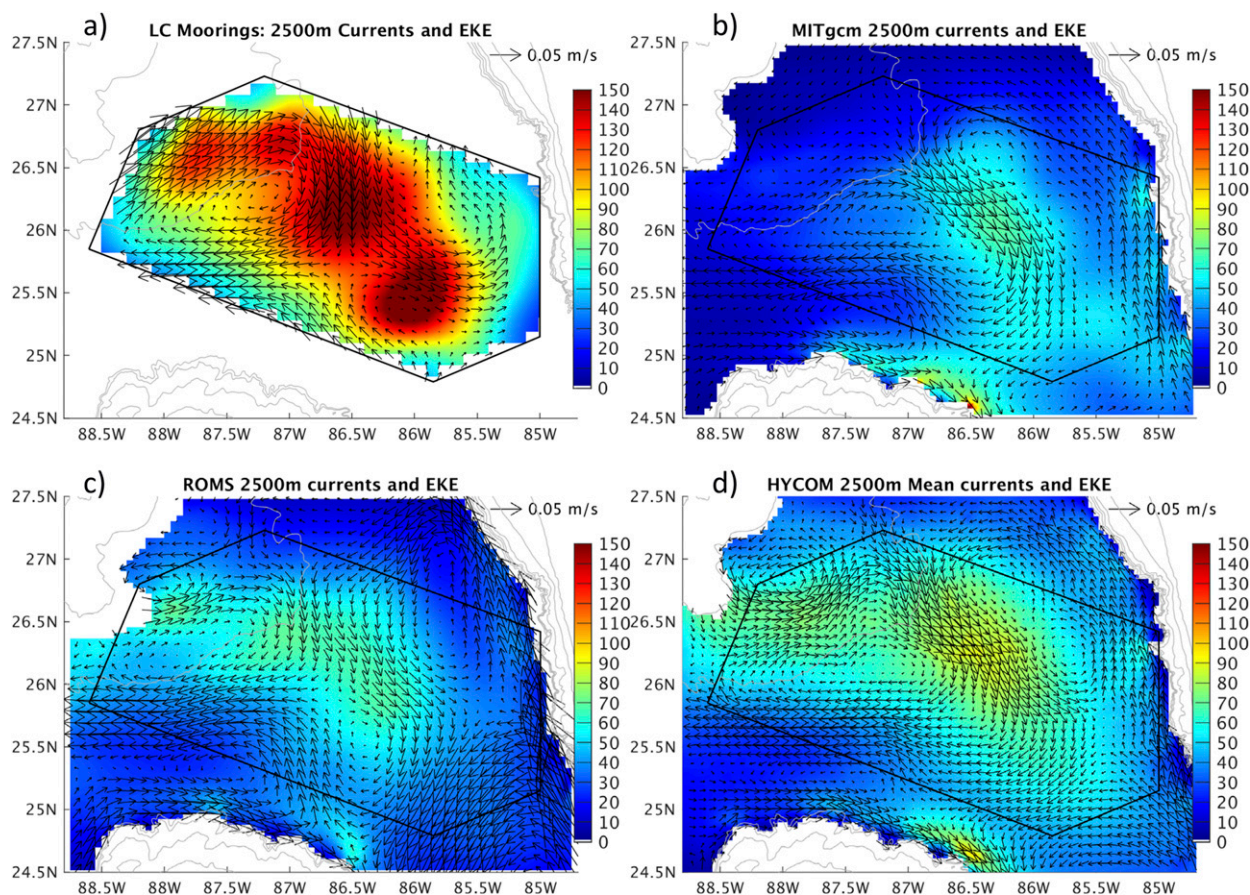The standard errors of the mean lower-layer velocity computed from the thirteen 4-yr records of the HYCOM

FIG. 6. EKE ($\text{cm}^2\,\text{s}^{-2}$) and mean velocity vectors at 2500 m from (a) mapped velocity fields from the Loop Current Study moorings (Hamilton et al. 2014) and the (b) MITgcm, (c) ROMS, and (d) HYCOM simulations. Model vectors are shown every second grid point.

simulation (blue ellipses in Fig. 2d) are small compared to the mean vector throughout much of the basin. The largest uncertainty in the mean velocity estimates are in the dipole feature and cyclonic circulation to its south in the eastern GoM. This analysis suggests that the Sigsbee Abyssal Gyre is well represented by its 4-yr mean, as is the boundary current, except for in the southeastern GoM where the cyclonic circulation appears as a recirculation of the boundary current. Thus, one should expect some variability in the structure of the dipole (or tripole, if the cyclone to the south of the dipole is considered) under the LC among different time periods comparable to the 4-yr record length. The deep dipole is likely an expression of deep eddies that lead the baroclinically unstable meanders propagating around the periphery of the LC and strengthening during periods of eddy separation as explained by Donohue et al. (2016b). Given the distribution of LC eddy separation periods with expected value of 8 months and maximum of 19 months from 18 years of altimeter observations (Dukhovskoy et al. 2015), it seems likely that LC and eddy

activity can vary among 4-yr time periods with impact on the estimate of the mean circulation. Nevertheless, the presence of the dipole-like structure seems to be ubiquitous in the mean velocity field computed from records of this length, albeit with some differences in its structure.

c. Eddy kinetic energy

Each of the models simulates weaker variability of currents in the deep layer of the GoM, as quantified by the EKE, than observed by the RAFOS floats (Fig. 4) and the Loop Current Study moorings (Fig. 6). The models all share the similar trait of generally enhanced EKE in the eastern part of the basin compared to the western part. This is similar to that shown by the EKE of the binned float velocities, but with reduced magnitude. EKE values exceed $100\,\text{cm}^2\,\text{s}^{-2}$ in certain locations under the LC as determined from the float data. The EKE computed from the mapped Loop Current Study mooring data shows even higher values, exceeding $150\,\text{cm}^2\,\text{s}^{-2}$, in the LC region (Fig. 6). Given the different time periods of mooring and Lagrangian measurements, it is not clear

whether this difference in EKE magnitude is due to differences in observational methods (e.g., instruments or platforms for current measurements), averaging period, or sampling. The models have maximum EKE values of approximately 60–75 cm^2 s^{-2} in this region, with HYCOM having the largest values (Figs. 4b–d). A region of elevated EKE extends westward from the LC region along the northern part of the deep basin in the ROMS simulation, where EKE values are comparable to those computed from the float data. The HYCOM simulation has a similar feature, yet it is weaker and more closely confined to the Sigsbee Escarpment. It is likely that this feature is due to TRWs radiating westward from the LC region (Hamilton 2007, 2009).

The standard error (or standard deviation serving as a proxy to the standard error) of EKE estimates from 4-yr records of the HYCOM simulation (Fig. 4e) is roughly 20%–40% of the EKE determined by averaging the EKE computed from the thirteen 4-yr model records. This relatively wide standard error points to significant differences in EKE among different 4-yr time periods and suggests that the highest EKE values computed from the float data are within the range of those that can be simulated by the models. The lower-layer EKE in the northeastern GoM is likely linked with how active the LC is during the sampling period, as shown by Donohue et al. (2016b).

Pérez-Brunius et al. (2018) noted a localized region of elevated EKE off the northwestern Campeche Bank around 91°W, to the northeast of a region of high MKE (Fig. 3a). Their inspection of individual trajectories revealed that some floats separated from the boundary current between these high MKE and EKE regions. Some of these floats then moved westward in deep anticyclonic eddies with estimated radii of 6–28 km (Furey et al. 2018), likely contributing to the elevated EKE signature. None of the models simulate this high EKE region in this location. This may be due to the eddies being of smaller scale than can be resolved by the model grids or by eddy generation linked with small-scale topographic features also not resolved in the smoothed model bathymetry. The HYCOM simulation has the highest resolution of the three models (4-km grid spacing), and does show a region of high MKE along the northwestern Campeche Bank in agreement with the analysis of the float data, but like the others, there is no evidence of a region of high EKE indicative of strong eddy activity here.

The ratio of MKE to the total kinetic energy is used by Pérez-Brunius et al. (2018) to give an indication of the relative persistence of the major circulation features of the deep GoM (Fig. 5a). The Sigsbee Abyssal Gyre is highlighted by larger values of this quantity due to its relative persistence (Fig. 5). Low values in the eastern GoM suggest that the eddy structure under the LC region is highly variable, and the dipole likely only exists in the mean velocity field. The cyclone to the south of this dipole feature is also highly variable, though the ROMS simulation appears to simulate this as a persistent structure (Fig. 5c). The cyclonic boundary flow also appears to be a transient feature around most of the basin evident only in the long-term mean. However, the MITgcm simulation simulates a more persistent southward flow along the western Bay of Campeche (Fig. 5b), and the ROMS simulation simulates a persistent boundary flow around all but the northern part of the GoM.

d. Comparison with velocity observations from moorings

Mean velocity vectors from the western GoM CANEK-group moorings show a cyclonically flowing circulation along the slope and mean velocity directions are consistent with the cyclonic Sigsbee Abyssal Gyre at the deepest mooring sites in the Bay of Campeche (Fig. 7). The similarity between mean and variability of velocity measured by the moored current meters and the gridded float velocities can be seen by comparing with Fig. 2a and is further illustrated and discussed in Pérez-Brunius et al. (2018).

Mean velocities from the MITgcm simulation at 1500-m depth (Fig. 7b) are generally similar to the observed currents in magnitude and direction, except over the northwestern slope. Here, the model mean currents are weaker than observed by the current meters or derived from the float trajectories (Fig. 2b). A striking feature of the variance ellipses of the MITgcm-simulated 1500 m currents is the stronger anisotropy compared to variability of observed currents over the steeper bathymetry (bathymetric gradients at the mooring locations are shown in Fig. 7a). This may be due to the representation of topography as stepwise in this z-level model (though this simulation uses shaved cells to mitigate these effects of the grid on the model topography by reducing step height). Dukhovskoy et al. (2006) discuss consequences of this type of grid on topographically trapped waves, showing that the stepwise bathymetry yields enhanced rectilinear velocity variability. Magnitudes of the variability are also smaller in the MITgcm-simulated currents compared to the current-meter observations over the slope. Over deeper water with smaller bathymetric gradients there is much better agreement in the simulated and observed current variability with very close match of the standard deviation ellipses at the LMP3500 and ARE3500 mooring locations. At the PER3500 location, the model mean velocity is nearly zero compared
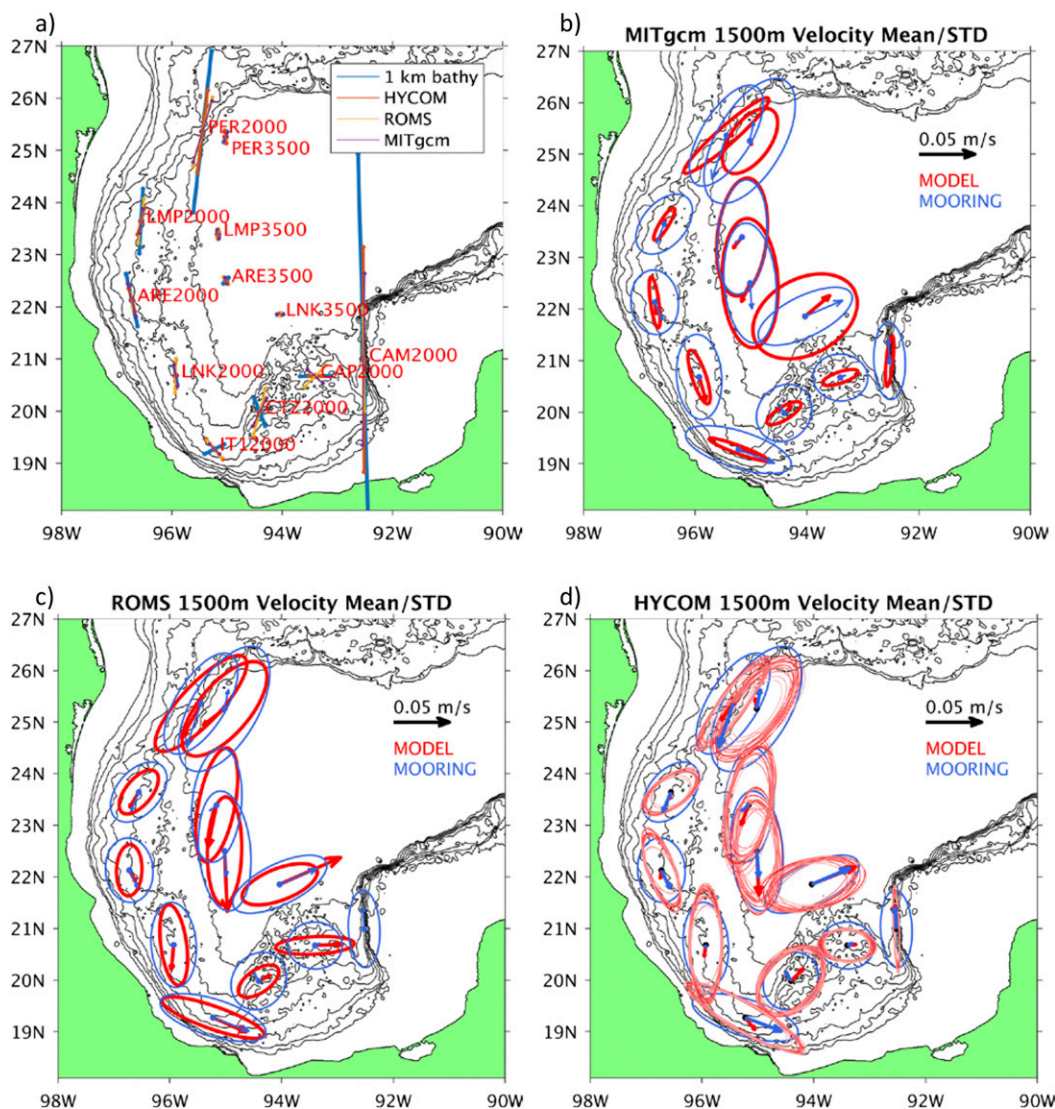
FIG. 7. Comparison between 4-yr statistics of (b) MITgcm, (c) ROMS, and (d) HYCOM model velocity with measured velocity (vertically interpolated from moored current-meter measurements as described in section 2). (a) Mooring locations, along with lines indicating the tangents to the local isobaths from an unfiltered 1-km-resolution bathymetry (Velissariou 2016) and each of the model bathymetry fields. The lengths of the lines indicate the relative magnitudes of the topographic gradients (computed as second-order centered differences for each bathymetry grid). Ellipses represent the standard deviation of velocity, and arrows represent the mean velocity. For the HYCOM simulation, standard deviation ellipses for each nonoverlapping 4-yr segment are drawn in different shades of pink/red, and the overall 52-yr mean velocity vectors are shown by the red arrows.

to a mean northward velocity from the current-meter measurements. The mean velocity derived from float trajectories at this location does not have a significant northward component, though, suggesting that this region may have either longer term variability such that this current-meter record is not long enough to accurately estimate the long-term mean (recall that at this location, the length of the data record is only 867 days as compared with 1460 days for the longest current-meter

records analyzed), or spatial variability due to small-scale flow features not resolved by the float data.

Mean velocity vectors from the ROMS simulation (Fig. 7c) are generally larger than from the other models and current-meter observations at most of the mooring locations (Fig. 2c). This is particularly evident at the deeper moorings around the western periphery of the Sigsbee Abyssal Gyre. Lack of agreement in mean velocity with the PER3500 observations is again evident

with this model, but this time with the ROMS simulation showing a mean southwestward current in contrast to the mean northward current from observations. Along the slope, variance ellipses are less eccentric than the MITgcm simulation and magnitudes of variability are more similar to observations, particularly in the southwestern Bay of Campeche (LNK2000 and ITI2000 moorings), and again match closely the observed variability at the LMP3500 and ARE3500 moorings. An exception is in the southern Bay of Campeche at CTZ2000 and CAP2000 where the model variance ellipses are much more anisotropic than the nearly isotropic observed variance. Note that the ROMS simulation has no 1500-m velocity data at the CAM2000 location because of smoothing of the model bathymetry over this very steep region (Fig. 7a).

Mean vectors from the entire 52 years (13 nonoverlapping 4-yr segments) of the HYCOM simulation are presented in Fig. 7d. As with the other model simulations, the presence of the cyclonic flow along the slope and the cyclonic flow along the western periphery of the Sigsbee Abyssal Gyre is well represented. Of all the model simulations, this HYCOM simulation is the only one to simulate a small mean northward velocity at 1500 m at the PER3500 mooring location, however the mean flow simulated over the slope is generally smaller than observed.

This multidecadal HYCOM simulation presents an opportunity to examine the uncertainty of estimates of the velocity variability computed from the 4-yr records, extending the analysis of the mean velocity fields and standard error ellipses (Fig. 2d) and the EKE standard error (Fig. 4e). Standard deviation ellipses computed from each of the thirteen 4-yr segments of the HYCOM simulation (Fig. 7d) are generally very similar suggesting that 4-yr observational records are long enough to provide good estimates of this statistic. The largest spread of the standard deviation ellipses between the thirteen 4-yr segments is seen at the deeper locations, along the Sigsbee Abyssal Gyre and most obviously at the PER3500 location. It is possible that variability at time scales of more than several years (e.g., occasional strong eddy impacts) affect the deep velocity statistics in the deep northwestern GoM, consistent with the suggestion by Tenreiro et al. (2018) that the propagation of LCEs over the western slope modulates the deep circulation.

The magnitudes and eccentricity of the ellipses computed from the HYCOM velocity match more closely the observations than do the other models. Notable exceptions are PER2000 and CAM2000 locations where the model variability is more rectilinear than observed, and ARE2000 where the model semimajor axis of the variance ellipse is rotated compared to observations. These discrepancies may be due to deficiencies in the

model representation of bathymetry. Model grid resolution and bathymetry smoothing lead to differences in local bathymetric gradients between the model bathymetry fields and an unfiltered high-resolution (1 km) bathymetric dataset, particularly over the rough bathymetry of the southern Bay of Campeche (Fig. 7a). Low frequency motions like TRWs, though, typically have length scales longer than the stencil over which the local gradients are computed from the high-resolution bathymetry (2 km using second-order centered differencing).

The KE spectra (Figs. 8 and 9) provide a means of comparing the energy at different frequencies between the models and the observed velocity time series. Spectral peaks in the CANEK (western GoM) current-meter velocity records at 25–40-day periods are prominent at several moorings located along the 2000-m isobath (ITI2000, PER2000, ARE2000, and LNK2000). Kolodziejczyk et al. (2011) analyzed the full mooring datasets at several of these locations and identified motions with similar periodicity as TRWs. The ROMS and HYCOM models also have spectral peaks near this frequency band at some of these locations suggesting that they are adequately simulating TRWs here. These motions are either lacking or very weak in the MITgcm simulation. Inspection of the spectra computed for each of the thirteen 4-yr segments (only one of which is shown in Figs. 8 and 9) shows substantial variability in the amount of energy contained in this frequency band. This also supports that there is low-frequency modulation of the TRW activity in the western GoM as discussed by Tenreiro et al. (2018).

Moving deeper, a similar spectral peak is seen at the PER3500 location, but energy is enhanced over a much broader band of periods (40–120 days) at the other 3500-m mooring locations. In contrast to the outer slope locations, here ROMS shows the weakest variability in this band compared to the other models. The HYCOM simulation has substantial energy at roughly 3-day periods at several locations. This is due to aliasing of nearinertial motions by analysis of the daily instantaneous model output.

In the eastern Gulf of Mexico, deep energy is dominated by TRWs and deep eddies resulting from baroclinic instabilities associated with the Loop Current (Hamilton et al. 2016a) evidenced by spectral peaks in the 20–100-day band. Secondary peaks are seen in the spectra from observed currents at roughly 15-day periods at the westernmost moorings (A1, A2, and B1). These may be associated with meanders along the western side of the LC. As expected from the EKE maps, HYCOM generally is the most energetic of the models. This model compares more favorably to the current-meter velocity spectra in the central part of
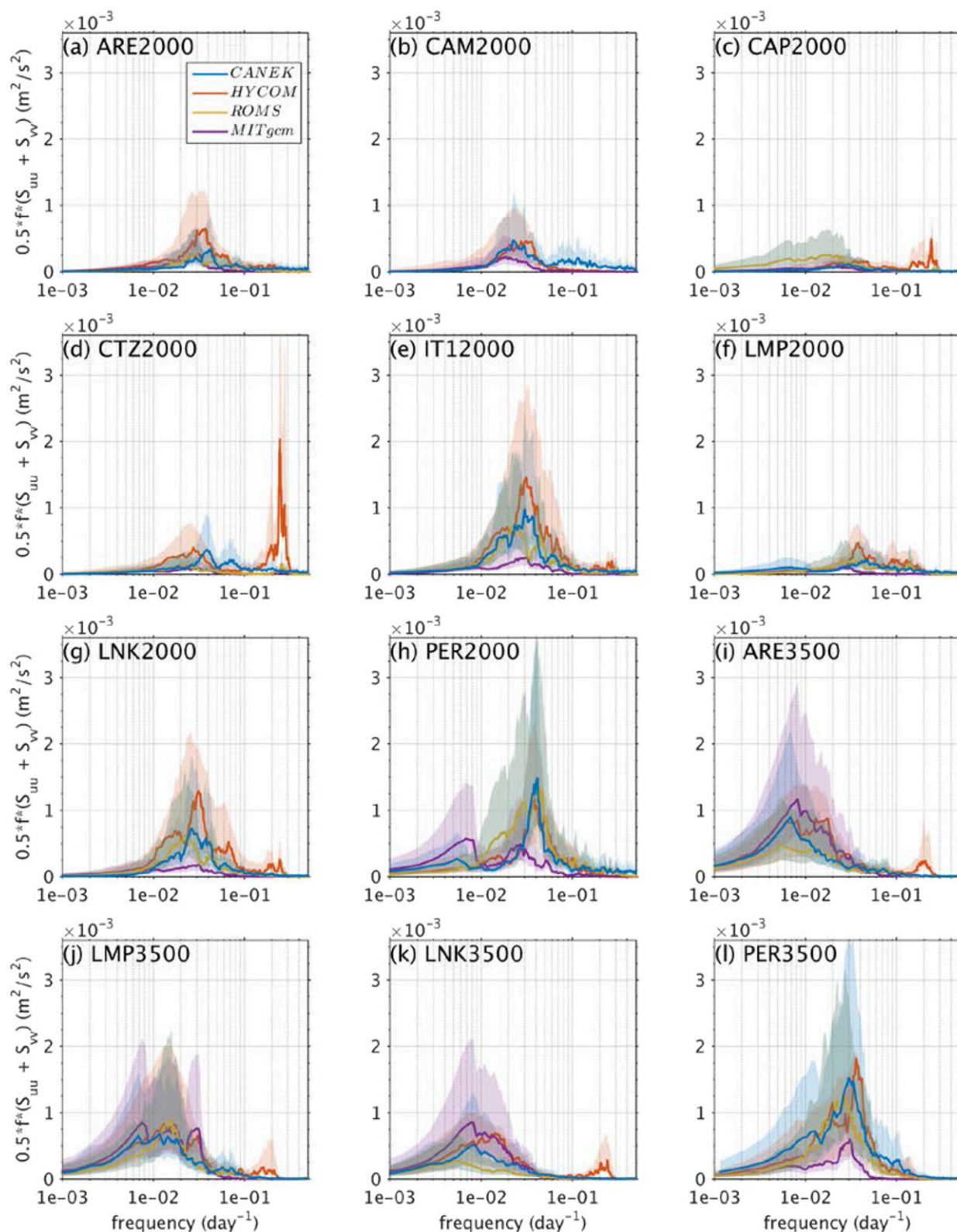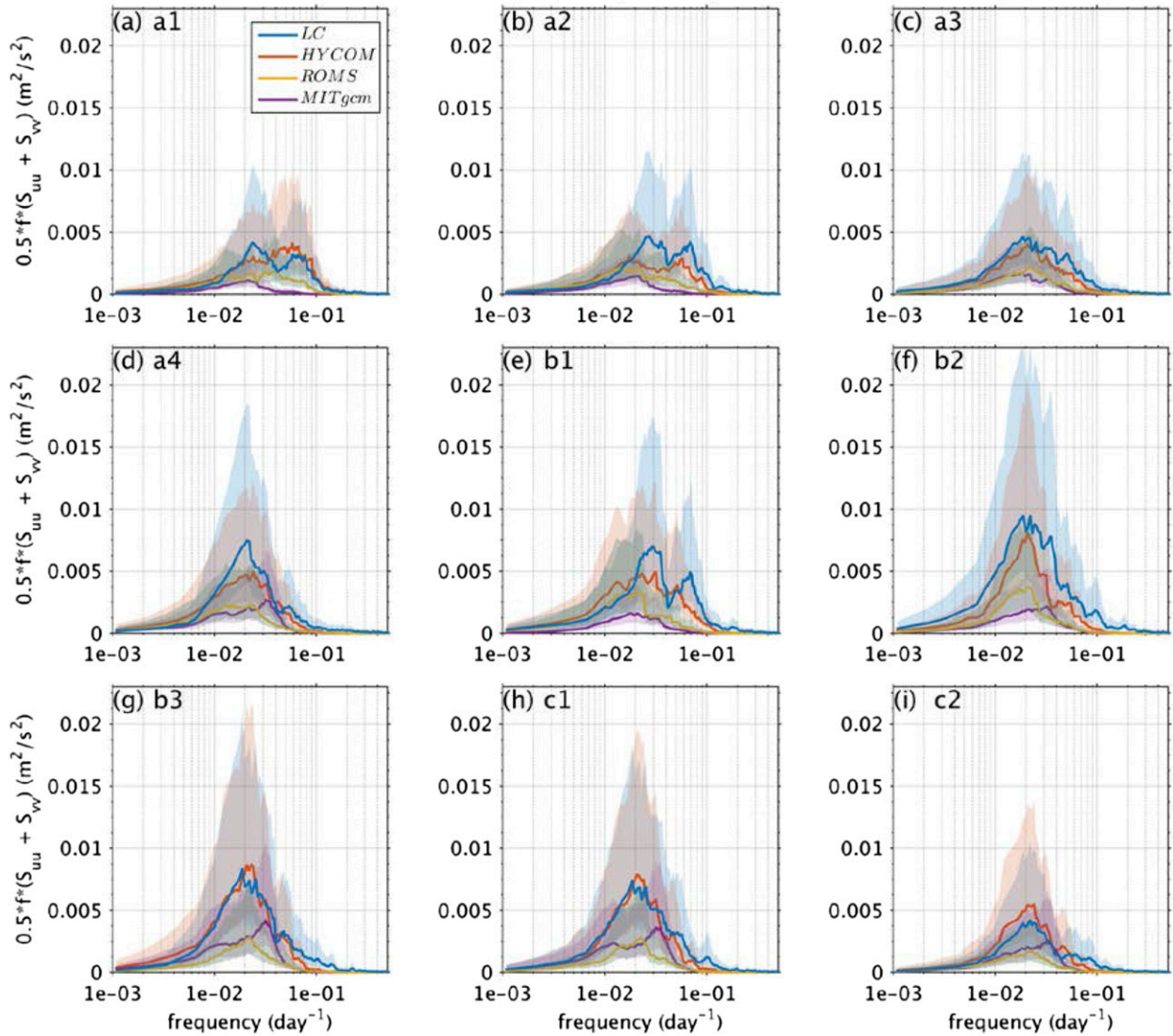
FIG. 8. Kinetic energy spectra for the 1500-m velocity time series measured and simulated at the western GoM mooring locations shown in Fig. 7a. Spectra are shown in variance-preserving form [0.5 × frequency × (S_{uu} + S_{vv}), where S_{uu} and S_{vv} are the autospectra for the eastward and northward velocity components]. Colored shading indicates the 95% confidence intervals. The spectra for the HYCOM simulation are plotted for only the first 4-yr segment. The "e" in the x-axis labels indicates that the value should be multiplied by 10 raised to the sign and numerals following it.

FIG. 9. Kinetic energy spectra for the 2000-m velocity time series measured and simulated at the Loop Current Study mooring locations shown in Fig. 1. Spectra are shown in variance-preserving form as described in Fig. 8.

the array (A3, B2, B3, and C1) than do the other models. Note that at some locations, the total variance is higher in the HYCOM velocity than observations, contrary to the lower EKE shown in Figs. 4 and 6. However, the EKE maps are produced using the entire 52-yr model record and the spectra displayed in Fig. 9 is from only one two-and-a-half-year segment of the model record and inspection of other time periods shows substantial variability among the spectra (thus, a low frequency modulation of the deep variability). The ROMS and MITgcm show substantially lower energy than the observations at all frequencies. The MITgcm shows a shift in the frequency of its maximum variance toward shorter periods, with peaks around 30 days at several mooring locations. The HYCOM simulation has a weak spectral

peak at 15-day period at A1 and A2, but the other models miss this observed feature.

4. Discussion and summary

Several recent extensive observational programs have allowed for the first time an assessment of how realistically numerical models simulate major features of the deep GoM circulation. Prior to these campaigns, inferences had to be made from limited observations to form a rather rudimentary and somewhat speculative depiction of the GoM-wide circulation below the upper layer. Because of the prior lack of knowledge of the major characteristics of the deep circulation, there has been much uncertainty in the value of numerical models

for studies of the deep GoM outside of certain well-observed locations (e.g., the Sigsbee Escarpment where extensive deep measurements have been made by the oil and gas industry) where model assessment was possible. Nevertheless, models have been used for a variety of studies of dispersal of biota and hydrocarbons at depth despite not knowing how well they represent reality. The recent observational programs and analyses of their data now provide a baseline for assessing models for use in studies such as these applications or of dynamical processes.

The major features of the mean deep circulation within the GoM from the recent observational programs are: the cyclonic Sigsbee Abyssal Gyre, the counter-rotating anticyclone–cyclone pair under the LC, the cyclonic circulation south of this feature (forming a tripole-like structure), and a cyclonic flow around perimeter of the basin along the outer slope. Each of the three free-running stochastic numerical simulations considered in this work simulate these mean circulation features in some manner, though with some differences in their structure, strength, and variability. From this most basic result of this work, one can infer that these commonly used models, when configured with realistic bathymetry and forced with throughflow producing realistic upper ocean LC and eddy features, have the dynamics necessary for forcing a realistic deep-layer circulation and thus have utility for studying dynamics of the coupling between the upper and deep layers of the GoM.

The analyses presented in this work do highlight, however, some important areas in which the models disagree with the observed deep circulation. These disagreements can have important implications for the application of these models for certain studies, such as predicting transport of pollutants and biota at depth and for prediction or estimation of mean and extreme deep currents impacting offshore structures. These results highlight areas in which the models may be improved through their configuration, numerics, parameterization, or with data assimilation. This will likely require a more extensive set of sensitivity experiments, but this is possible now given targets for the model solution to achieve and a baseline of the models' capabilities. It is likely that many of these issues are fundamentally linked to the types of vertical grids used by the models, the horizontal resolution of the model configurations, and effective bathymetry resolution (by sampling and smoothing) given constraints by model numerics and grid resolution. A striking example is the lack of a spectral peak at frequencies associated with TRWs in the western GoM in the MITgcm simulation. Having the coarsest resolution in this region at 10 km and using a z-level vertical coordinate, it is likely that refinements in

both the horizontal and vertical resolution will allow this model to better reproduce these features (Dukhovskoy et al. 2006).

Assessment of the deep circulation simulated by these numerical models is a fundamentally important step toward improving ocean prediction (primarily Loop Current and upper ocean eddy evolution) through advances in assimilation of surface ocean observations (including satellite data) using techniques that project this information throughout the water column, as well as assimilation of new measurements within the deep layer of the GoM. Analysis of the performance of the free-running simulations at depth provides a baseline for evaluating data-assimilative versions of these models, as it can now be assessed whether or not the data assimilation techniques actually improve the model representation of the deep currents. Rosburg et al. (2016) compared deep circulation from these measurements to a data assimilative Gulf of Mexico HYCOM simulation. While the model reproduced some basic features of the upper layer–deep layer coupling associated with meanders in the LC, the data assimilative HYCOM mean deep currents did not reveal such a clear expression of the dipole structure. The authors also reported that the model EKE at 2500-m depth was approximately one-half of that observed over this region. Further studies with assimilation of a recently deployed larger array of moorings under the Loop Current region (National Academies of Sciences Engineering and Medicine 2018) will provide knowledge of the value of these deep observations for GoM forecasting.

data are available from the HYCOM data server (https://www.hycom.org/data/goml0pt04/expt-02pt2), MITgcm data are available from the ECCO data server (http://ecco.ucsd.edu/gom_results2.html), and the ROMS simulation data are available from GRIIDC (NA.x837.000:0001).

REFERENCES

Chassignet, E. P., and Z. D. Garraffo, 2001: Viscosity parameterization and the Gulf Stream separation. *From Stirring to Mixing in a Stratified Ocean: Proc. 12th 'Aha Huliko'a Hawaiian Winter Workshop*, Honolulu, HI, University of Hawai'i at Mānoa, 37–41.

——, H. E. Hurlburt, O. M. Smedstad, G. R. Halliwell, P. J. Hogan, A. J. Wallcraft, R. Baraille, and R. Bleck, 2007: The HYCOM (Hybrid Coordinate Ocean Model) data assimilative system. *J. Mar. Syst.*, **65**, 60–83, https://doi.org/10.1016/j.jmarsys.2005.09.016.

——, and Coauthors, 2009: US GODAE: Global ocean prediction with the Hybrid Coordinate Ocean Model (HYCOM). *Oceanography*, **22** (2), 64–75, https://doi.org/10.5670/oceanog.2009.39.

DeHaan, C. J., and W. Sturges, 2005: Deep cyclonic circulation in the Gulf of Mexico. *J. Phys. Oceanogr.*, **35**, 1801–1812, https://doi.org/10.1175/JPO2790.1.

Donohue, K. A., D. R. Watts, P. Hamilton, R. Leben, and M. Kennelly, 2016a: Gulf of Mexico Loop Current path variability. *Dyn. Atmos. Oceans*, **76**, 174–194, https://doi.org/10.1016/j.dynatmoce.2015.12.003.

——, ——, ——, and ——, 2016b: Loop Current eddy formation and baroclinic instability. *Dyn. Atmos. Oceans*, **76**, 195–216, https://doi.org/10.1016/j.dynatmoce.2016.01.004.

Dukhovskoy, D. S., S. L. Morey, and J. J. O'Brien, 2006: Influence of multi-step topography on barotropic waves and consequences for numerical modeling. *Ocean Modell.*, **14**, 45–60, https://doi.org/10.1016/j.ocemod.2006.03.002.

——, ——, ——, P. J. Martin, and C. Cooper, 2009: Application of a vanishing quasi-sigma vertical coordinate for simulation of high-speed deep currents over the Sigsbee Escarpment in the Gulf of Mexico. *Ocean Modell.*, **28**, 250–265, https://doi.org/10.1016/j.ocemod.2009.02.009.

——, R. R. Leben, E. P. Chassignet, C. A. Hall, S. L. Morey, and R. Nedbor-Gross, 2015: Characterization of the uncertainty of Loop Current metrics using a multidecadal numerical simulation and altimeter observations. *Deep-Sea Res. I*, **100**, 140–158, https://doi.org/10.1016/j.dsr.2015.01.005.

Egbert, G. D., and S. Y. Erofeeva, 2002: Efficient inverse modeling of barotropic ocean tides. *J. Atmos. Oceanic Technol.*, **19**, 183–204, https://doi.org/10.1175/1520-0426(2002)019<0183:EIMOBO>2.0.CO;2.

Emery, W. J., and R. E. Thomson, 2004: *Data Analysis Methods in Physical Oceanography*. Elsevier, 638 pp.

Estrada-Allis, S. N., J. Sheinbaum Pardo, J. M. Azevedo Correia de Souza, J. Sheinbaum Pardo, C. E. Enríquez Ortiz, I. M. Mariño Tapia, and J. A. Herrera-Silveira, 2020: Dissolved inorganic nitrogen and particulate organic nitrogen budget in the Yucatán shelf: Driving mechanisms through a physical–biogeochemical coupled model. *Biogeosciences*, **17**, 1087–1111, https://doi.org/10.5194/bg-17-1087-2020.

Furey, H., A. Bower, P. Perez-Brunius, P. Hamilton, and R. Leben, 2018: Deep eddies in the Gulf of Mexico observed with Floats. *J. Phys. Oceanogr.*, **48**, 2703–2719, https://doi.org/10.1175/JPO-D-17-0245.1.

Gopalakrishnan, G., B. D. Cornuelle, and I. Hoteit, 2013a: Adjoint sensitivity studies of Loop Current and eddy shedding in the Gulf of Mexico. *J. Geophys. Res. Oceans*, **118**, 3315–3335, https://doi.org/10.1002/jgrc.20240.

——, ——, ——, D. L. Rudnick, and W. B. Owens, 2013b: State estimates and forecasts of the Loop Current in the Gulf of Mexico using the MITgcm and its adjoint. *J. Geophys. Res. Oceans*, **118**, 3292–3314, https://doi.org/10.1002/jgrc.20239.

——, I. Hoteit, B. D. Cornuelle, and D. L. Rudnick, 2019: Comparison of 4DVAR and EnKF state estimates and forecasts in the Gulf of Mexico. *Quart. J. Roy. Meteor. Soc.*, **145**, 1354–1376, https://doi.org/10.1002/qj.3493.

Gravetter, F. J., and L. B. Wallnau, 2014: *Essentials of Statistics for the Behavioral Sciences*. 8th ed. Wadsworth, 648 pp.

Haidvogel, D. B., and Coauthors, 2008: Ocean forecasting in terrain-following coordinates: Formulation and skill assessment of the Regional Ocean Modeling System. *J. Comput. Phys.*, **227**, 3595–3624, https://doi.org/10.1016/j.jcp.2007.06.016.

Hamilton, P., 1990: Deep currents in the Gulf of Mexico. *J. Phys. Oceanogr.*, **20**, 1087–1104, https://doi.org/10.1175/1520-0485(1990)020<1087:DCITGO>2.0.CO;2.

——, 2007: Deep current variability near the Sigsbee Escarpment in the Gulf of Mexico. *J. Phys. Oceanogr.*, **37**, 708–726, https://doi.org/10.1175/JPO2998.1.

——, 2009: Topographic Rossby waves in the Gulf of Mexico. *Prog. Oceanogr.*, **82**, 1–31, https://doi.org/10.1016/j.pocean.2009.04.019.

——, and A. Lugo-Fernandez, 2001: Observations of high speed deep currents in the northern Gulf of Mexico. *Geophys. Res. Lett.*, **28**, 2867–2870, https://doi.org/10.1029/2001GL013039.

——, K. Donohue, C. Hall, R. R. Leben, H. Quian, J. Sheinbaum, and D. R. Watts, 2014: Observations and dynamics of the Loop Current. Rep. BOEM 2015-006, 389 pp., https://digital.library.unt.edu/ark:/67531/metadc955416/m1/1/.

——, A. Lugo-Fernández, and J. Sheinbaum, 2016a: A Loop Current experiment: Field and remote measurements. *Dyn. Atmos. Oceans*, **76**, 156–173, https://doi.org/10.1016/j.dynatmoce.2016.01.005.

——, A. Bower, H. Furey, R. R. Leben, and P. Peìrez-Brunius, 2016b: Deep circulation in the Gulf of Mexico: A Lagrangian study. U.S. Dept. of the Interior Bureau of Ocean Energy Management Rep. BOEM 2016-081, 273 pp., https://permanent.access.gpo.gov/gpo80279/5583%5b1%5d.pdf.

——, ——, ——, R. Leben, and P. Peìrez-Brunius, 2019: The Loop Current: Observations of deep eddies and topographic waves. *J. Phys. Oceanogr.*, **49**, 1463–1483, https://doi.org/10.1175/JPO-D-18-0213.1.

Hofmann, E. E., and S. J. Worley, 1986: An investigation of the circulation of the Gulf of Mexico. *J. Geophys. Res.*, **91**, 14 221–14 236, https://doi.org/10.1029/JC091iC12p14221.

Hoteit, I., T. Hoar, G. Gopalakrishnan, N. Collins, J. Anderson, B. Cornuelle, A. Köhl, and P. Heimbach, 2013: A MITgcm/DART ensemble analysis and prediction system with application to the Gulf of Mexico. *Dyn. Atmos. Oceans*, **63**, 1–23, https://doi.org/10.1016/j.dynatmoce.2013.03.002.

Hurlburt, H. E., and J. D. Thompson, 1980: A numerical study of Loop Current intrusions and eddy shedding. *J. Phys. Oceanogr.*, **10**, 1611–1651, https://doi.org/10.1175/1520-0485(1980)010<1611:ANSOLC>2.0.CO;2.

Kalnay, E., and Coauthors, 1996: The NCEP/NCAR 40-Year Reanalysis Project. *Bull. Amer. Meteor. Soc.*, **77**, 437–471, https://doi.org/10.1175/1520-0477(1996)077<0437:TNYRP>2.0.CO;2.

Kolodziejczyk, N., J. Ochoa, J. Candela, and J. Sheinbaum, 2011: Deep currents in the Bay of Campeche. *J. Phys. Oceanogr.*, **41**, 1902–1920, https://doi.org/10.1175/2011JPO4526.1.

——, ——, ——, and ——, 2012: Observations of intermittent deep currents and eddies in the Gulf of Mexico. *J. Geophys. Res.*, **117**, C09014, https://doi.org/10.1029/2012JC007890.

Marshall, J., A. Adcroft, C. Hill, L. Perelman, and C. Heisey, 1997: A finite-volume, incompressible Navier Stokes model for studies of the ocean on parallel computers. *J. Geophys. Res.*, **102**, 5753–5766, https://doi.org/10.1029/96JC02775.

Maslo, A., J. M. A. C. Souza, P. P. Brunius, and F. A. Canto, 2020: Connectivity of deep waters in the Gulf of Mexico. *J. Mar. Syst.*, **203**, 103267, https://doi.org/10.1016/j.jmarsys.2019.103267.

Metzger, E. J., and Coauthors, 2014: US Navy operational global ocean and Arctic ice prediction systems. *Oceanography*, **27**, 32–43, https://doi.org/10.5670/oceanog.2014.66.

Miron, P., F. J. Beron-Vera, M. J. Olascoaga, G. Froyland, P. Pérez-Brunius, and J. Sheinbaum, 2019: Lagrangian geography of the deep Gulf of Mexico. *J. Phys. Oceanogr.*, **49**, 269–290, https://doi.org/10.1175/JPO-D-18-0073.1.

Morey, S. L., and D. S. Dukhovskoy, 2013: A downscaling method for simulating deep current interactions with topography – Application to the Sigsbee Escarpment. *Ocean Modell.*, **69**, 50–63, https://doi.org/10.1016/j.ocemod.2013.05.008.

National Academies of Sciences, Engineering, and Medicine, 2018: *Understanding and Predicting the Gulf of Mexico Loop Current: Critical Gaps and Recommendations*. The National Academies Press, 116 pp., https://doi.org/10.17226/24823.

Nowlin, W. D., Jr., A. E. Jochens, S. F. DiMarco, R. O. Reid, and M. K. Howard, 2001: Deepwater physical oceanography reanalysis and synthesis of historical data: Synthesis report. U.S. Dept. of the Interior Minerals Management Service OCS Study Tech. Rep. MMS 2001-064, 528 pp., https://ntrl.ntis.gov/NTRL/dashboard/searchResults/titleDetail/PB2005102079.xhtml.

Oey, L.-Y., 2008: Loop Current and deep eddies. *J. Phys. Oceanogr.*, **38**, 1426–1449, https://doi.org/10.1175/2007JPO3818.1.

Pallàs-Sanz, E., J. Candela, J. Sheinbaum, J. Ochoa, and J. Jouanno, 2016: Trapping of the near-inertial wave wakes of two consecutive hurricanes in the Loop Current. *J. Geophys. Res. Oceans*, **121**, 7431–7454, https://doi.org/10.1002/2015JC011592.

Pérez-Brunius, P., H. Furey, A. Bower, P. Hamilton, J. Candela, P. García-Carrillo, and R. Leben, 2018: Dominant circulation patterns of the deep Gulf of Mexico. *J. Phys. Oceanogr.*, **48**, 511–529, https://doi.org/10.1175/JPO-D-17-0140.1.

Rosburg, K. C., K. A. Donohue, and E. P. Chassignet, 2016: Three-dimensional model-observation comparison in the Loop Current region. *Dyn. Atmos. Oceans*, **76**, 283–305, https://doi.org/10.1016/j.dynatmoce.2016.05.001.

Rudnick, D. L., G. Gopalakrishnan, and B. D. Cornuelle, 2015: Cyclonic eddies in the Gulf of Mexico: Observations by underwater gliders and simulations by numerical model. *J. Phys. Oceanogr.*, **45**, 313–326, https://doi.org/10.1175/JPO-D-14-0138.1.

Saha, S., and Coauthors, 2010: The NCEP Climate Forecast System reanalysis. *Bull. Amer. Meteor. Soc.*, **91**, 1015–1058, https://doi.org/10.1175/2010BAMS3001.1.

Shchepetkin, A. F., and J. C. McWilliams, 2003: A method for computing horizontal pressure-gradient forcing in an oceanic model with a nonaligned vertical coordinate. *J. Geophys. Res.*, **108**, 3090, https://doi.org/10.1029/2001JC001047.

——, and ——, 2005: The regional oceanic modeling system (ROMS): A split-explicit, free-surface, topography-following-coordinate oceanic model. *Ocean Modell.*, **9**, 347–404, https://doi.org/10.1016/j.ocemod.2004.08.002.

——, and ——, 2009: Correction and commentary for "Ocean forecasting in terrain-following coordinates: Formulation and skill assessment of the regional ocean modeling system" by Haidvogel et al., J. Comp. Phys. 227, pp. 3595–3624. *J. Comput. Phys.*, **228**, 8985–9000, https://doi.org/10.1016/j.jcp.2009.09.002.

Sheinbaum, J., A. Badan, J. Ochoa, J. Candela, D. Rivas, and J. I. González, 2007: Full water column current observations in the central Gulf of Mexico. U.S. Dept. of the Interior Minerals Management Service OCS Study Tech. Rep. MMS 2007-022, 58 pp.

Sikirić, M. D., I. Janeković, and M. Kuzmić, 2009: A new approach to bathymetry smoothing in sigma-coordinate ocean models. *Ocean Modell.*, **29**, 128–136, https://doi.org/10.1016/j.ocemod.2009.03.009.

Smolarkiewicz, P. K., and W. W. Grabowski, 1990: The multidimensional positive definite advection transport algorithm: Nonoscillatory option. *J. Comput. Phys.*, **86**, 355–375, https://doi.org/10.1016/0021-9991(90)90105-A.

Souza, J. M. A. C., B. Powell, A. C. Castillo-Trujillo, and P. Flament, 2015: The vorticity balance of the ocean surface in Hawaii from a regional reanalysis. *J. Phys. Oceanogr.*, **45**, 424–440, https://doi.org/10.1175/JPO-D-14-0074.1.

Stammer, D., and Coauthors, 2002: The global ocean circulation during 1992–1997, estimated from ocean observations and a general circulation model. *J. Geophys. Res.*, **107**, 3118, https://doi.org/10.1029/2001JC000888.

Tenreiro, M., J. Candela, E. Pallàs-Sanz, J. Sheinbaum, and J. Ochoa, 2018: Near-surface and deep circulation coupling in the western Gulf of Mexico. *J. Phys. Oceanogr.*, **48**, 145–161, https://doi.org/10.1175/JPO-D-17-0018.1.

Velissariou, P., 2016: Gulf of Mexico high-resolution (0.01° × 0.01°) bathymetric grid—version 2.0, February 2013. Deep Sea to Coast Connectivity in the Eastern Gulf of Mexico (DEEP-C), accessed 22 November 2019, https://doi.org/10.7266/N7X63JZ5.

Vukovich, F. M., 2007: Climatology of ocean features in the Gulf of Mexico using satellite remote sensing data. *J. Phys. Oceanogr.*, **37**, 689–707, https://doi.org/10.1175/JPO2989.1.